Journal Pre-proofs


# Accelerating pharmaceutical tablet development by transfer of powder compaction equipment across types and scales

Luca Beccaro, Pierantonio Facco, Ranjit M. Dhenge, Marv J. Khala, Francesca Cenci, Fabrizio Bezzo, Massimiliano Barolo

PII: S0378-5173(24)01138-4
DOI: https://doi.org/10.1016/j.ijpharm.2024.124904
Reference: IJP 124904

To appear in: *International Journal of Pharmaceutics*

Received Date: 24 July 2024
Revised Date: 29 October 2024
Accepted Date: 1 November 2024

Please cite this article as: L. Beccaro, P. Facco, R.M. Dhenge, M.J. Khala, F. Cenci, F. Bezzo, M. Barolo, Accelerating pharmaceutical tablet development by transfer of powder compaction equipment across types and scales, *International Journal of Pharmaceutics* (2024), doi: https://doi.org/10.1016/j.ijpharm.2024.124904

# Accelerating pharmaceutical tablet development by transfer of powder compaction equipment across types and scales

Luca Beccaro[1], Pierantonio Facco[1], Ranjit M. Dhenge[2], Marv J. Khala[3,†], Francesca Cenci[3], Fabrizio Bezzo[1], and Massimiliano Barolo[1,*]

[1]*CAPE-Lab – Computer-Aided Process Engineering Laboratory*

*Department of Industrial Engineering*

*University of Padova*

*via Marzolo 9, 35131 Padova PD (Italy)*

[2]*GSK Global Supply Chain, Priory Street, Ware SG12 0DJ, UK*

[3]*GSK Ware Research and Development, Park Road, SG12 0DP, Ware, UK*

Submitted to: *International Journal of Pharmaceutics*



† Currently at AstraZeneca (U.K.)

* Corresponding author: max.barolo@unipd.it

Original manuscript submitted on July 24, 2024

First revision submitted on October 2, 2024

**Second revision submitted on October 29, 2024**

## Abstract

Roller compaction is a key unit operation in a dry granulation line for pharmaceutical tablet manufacturing. During product development, one would like to find the roller compactor (RC) settings that are required to achieve a desired ribbon solid fraction. These settings can be determined from the compression profile of the powder mixture being compacted and a mathematical model that interprets it. However, establishing compression profiles in an RC requires relatively large amounts of powder, which are expensive and may not be available during drug development. As a cost-effective alternative to an RC, a compactor simulator (CS) can be used, which is a small-scale equipment that uses minimal amounts of powder to build the compression profile. However, since the working principles of a CS and an RC are different, the compression profiles obtained from the two devices for a given powder are also different. In this study, we propose a transfer learning approach that allows the RC compression profile of a given powder to be easily predicted from the compression profile obtained in a CS for the same powder. Based on the well-known Johanson model and on the mass correction factor theory, we examine the compaction behavior of six formulations, two of which including active ingredients, and we find that the mass correction factor does not depend significantly on the powder being compacted. We develop a simple, generalized correlation (transfer model) that allows the mass correction factor to be predicted solely as a function of the pressure at which the compaction is carried out. By using the proposed transfer model, the prediction of the RC compression profiles for the validation powders is significantly improved over the case where a constant value of the mass correction factor is used.

**Keywords**: roller compaction; tablet manufacturing; transfer learning; Johanson model; compactor simulation; mass correction factor; pharmaceutical tablets

## 1 Introduction

Roll compaction is a continuous dry granulation method used to produce solid oral-dosage forms from powder blends (Leane et al., 2015; Bano et al., 2022). This process is employed to induce pressure-driven agglomeration within the pharmaceutical blend, resulting in the formation of granules that exhibit enhanced homogeneity in the distribution of components and particle size, and better flowability (Guigon et al., 2007; Reynolds, 2019; Kleinebudde, 2022). The use of this technique has become increasingly popular over wet granulation, as it eliminates the need for solvents or liquid binders, as well as the subsequent drying procedure to remove the latter. This is particularly advantageous for heat- and moisture-sensitive active pharmaceutical ingredients (APIs) (Adeyeye, 2000; Kleinebudde, 2004).

In roll compaction, the powder blend is moved between two adjustable counter-rotating rollers, which apply pressure to compress and densify the powder, resulting in the formation of a consolidated mass known as the ribbon. The latter is subsequently milled into granules that undergo additional blending and lubrication before being compressed into tablets. The ribbon solid fraction (SF) is a critical quality attribute, since it significantly impacts the downstream properties of the granules and, subsequently, the finished tablets (Gavi and Reynolds, 2014; Sun and Kleinebudde, 2016). The ribbon SF is mainly determined by the frictional properties and compressibility behavior of the feed powder material, as well as by the roller compactor (RC) geometry and operating parameters (Hassan et al., 2023).

To quantitatively describe the interplay between materials properties, machine parameters and ribbon SF in roll compaction, a mathematical model is required (Dec et al., 2003; Muthancheri et al., 2024).

Johanson (1965) introduced a mechanics rolling theory for granular solids which can provide predictions of the roll normal stress distribution, roll torque, and ribbon density at the minimum roll gap as a function of the powder properties, RC geometry and RC operating parameters. Despite its many simplifications and assumptions, the Johanson model has emerged as the most widely used one due to its remarkable prediction accuracy and straightforward computational approach (Bindhumadhavan et al., 2005). The parameters of the Johanson model are formulation-specific and can be estimated from compression profiles, namely profiles of ribbon SF at different values of the maximum pressure applied by the RC. However, determination of the compression profile in RC equipment requires considerable amounts of material, especially of API that is expensive and might be scarcely available at the drug development stage. Use of small-scale (pilot) RCs, instead of full-scale ones, mitigates the problem, but does not eliminate it (Desai et al., 2024; Pérez Gago et al., 2018).

Zinchuk et al. (2004) addressed this problem by developing a compactor simulator (CS), namely, a technique for simulating the compaction phenomena observed during roller compaction using uniaxial die compaction. In a CS, the sinusoidal displacement profile of two punches replicates the displacement of a specific point on the surface of the rollers. The primary benefit of a CS is its capacity to investigate and quantify compressibility and compactability using only one tablet's worth of material for each single experiment repetition, therefore allowing for significant materials savings. However, the compression process in a die is characterized by a stress path that follows hydrostatic stress, which is not the same path exhibited by roll compaction, where shear stress prevails (Farber et al., 2008). This makes the compression profile obtained from a CS different from the one obtained from an RC for the same powder.

The transfer of compaction equipment across scales is a key issue in the development of solid oral dosage forms (Reynolds et al., 2010; Nesarikar et al., 2012; Rowe et al., 2017). Bi et al. (2014) introduced a Johanson model correction parameter, called the mass correction factor, which allowed the compression profiles obtained in an RC and in a CS to be related. They considered three different powder mixtures including the same API, and they found that the mass correction factor was sensitive to the powder material properties (i.e., to the powder composition); however, they were unable to provide a relation to predict the mass correction factor. So et al. (2021) determined the mass correction factor for three pharmaceutical excipients of diverse compressibility and concluded that the mass correction factor can be characterized by a unique value for the three excipients at any operating conditions. They proposed an approach called virtual RC, i.e., a predictive model that allows one to predict the ribbon SF in an RC given the roll force, the roll gap width, and the powder compressibility as measured from experiments conducted in a CS. However, whether or not their findings hold true also for other excipients or for mixtures including an API is still an open issue.

Amini and Akseli (2020) used CS compression profiles to infer compressibility information for the RC. The approach proved accurate for placebo and active ingredient formulations using minimal amounts of materials, but within a pressure range than may be affected by the powder mixture composition. Sato et al. (2024) developed a gray-box (first-principles + statistical) model that enabled describing the impact of process parameters and material attributes on ribbon density by using small-scale uniaxial compression tests. However, the hybrid model is complex to design and does not perform well for mixtures with high compressibility; furthermore, only formulations not including APIs were used. Reimer and Kleinebudde (2019) proposed a hybrid methodology based on a correction factor that allows the experimental profiles obtained from small-scale and large-scale equipment to be correlated. They used the thin layer model to describe the CS experimental data, rather than the more popular Johanson model, and their results are limited to two excipients.

In this study, building on the studies of Bi et al. (2014) and So et al. (2021), we propose a workflow that exploits the concepts of mass correction factor and virtual RC to predict the RC compression profile for a given powder mixture by carrying out experiments solely on a CS. We analyze the

compaction behavior of six powder mixtures, two of which including API's, and we develop and validate a simple, generalized correlation that is able to predict the mass correction factor for a powder mixture (also containing an API) at different operating conditions, thus allowing the compression profile obtained in a CS to be accurately transferred to an RC compression profile.

The remainder of this paper is organized as follows. Section 2 serves as a background source of information on roll compaction modeling. The powder mixtures considered in the study, the experimental procedures in the RC and CS and the procedure to estimate the Johanson model parameters are presented in Section 3. The proposed transfer methodology is illustrated in Section 4, with reference to its design/calibration, validation and usage steps. Section 6 presents and discusses the results of the study, and a final section presents the conclusions.

# 2 Background on roll compaction modeling

## *2.1 Johanson's roller compaction model*

According to Johanson (1965), the area between rolls is split into two portions: the slip region, where slip occurs along the roll surface, and the nip region, where a no-slip boundary condition applies. The transition from slip to nonslip region defines the nip angle $\alpha$, i.e., the angular location along the roll surface at which the powder begins to move at the velocity of the roll, as illustrated in Figure 1. The zone beyond the minimum roll gap is usually defined as the release region in which the stresses are relieved, and the compacts are extruded from the system.

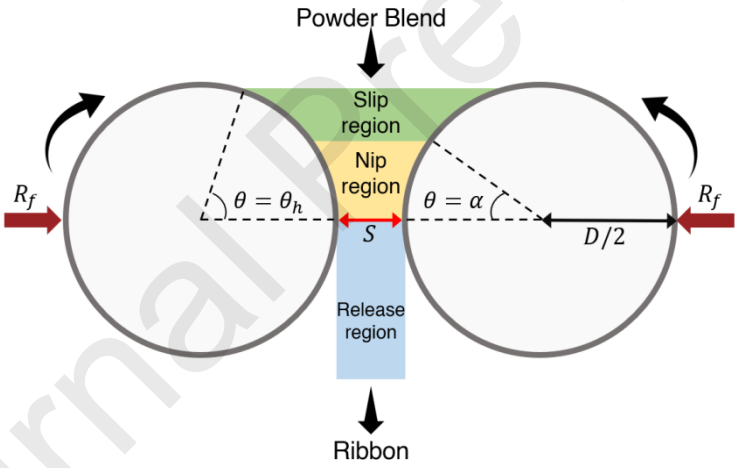


**Figure 1.** *Schematic of the roller compaction process and its characteristic regions*

To describe the powder behavior in the slip region, Johanson developed a model on the basis of the Jenike and Shield (1959) criterion for steady-state particle flow in silos and hoppers. The roll compacted material is assumed to be isotropic, frictional, cohesive and compressible, and also to obey the effective yield function proposed by Jenike and Shield (1959). Given the boundary conditions, one can obtain a first-order approximation of the pressure gradient ($\mathrm{d}\sigma/\mathrm{d}x$) in the slip region using the effective yield function as:

$$\left.\frac{d\sigma}{dx}\right|_{slip} = \frac{4\sigma\left(\frac{\pi}{2} - \theta - \nu\right)\tan\delta_E}{\frac{D}{2}\left[1 + \frac{S}{D} - \cos\theta\right]\left[\cot(A-\mu) - \cot(A+\mu)\right]} \quad , \tag{1}$$

where: $\theta$ is the angular position in radians, such that $\theta = 0$ corresponds to the minimum gap; $S$ and $D$ represent the rolls gap and diameter respectively; $x$ is the vertical distance upstream from the roll gap; $\delta_E$ is the effective angle of internal friction in degree; and the parameter $A$ is given by:

$$A = \frac{\theta + \nu + \frac{\pi}{2}}{2} \quad . \tag{2}$$

In (1), $\mu$ represents the friction coefficient of the material, and is given by:

$$\mu = \frac{\pi}{4} - \frac{\delta_E}{2} \quad . \tag{3}$$

In (1) and (2), $\nu$ represents the acute angle between major principal axis and tangent to roll surface, defined as:

$$2\nu = \pi - \arcsin\left(\frac{\sin\phi_W}{\sin\delta_E}\right) - \phi_W \quad , \tag{4}$$

where $\phi_W$ is the angle of wall friction. The decrease in available volume during the descent of the powder leads to an increase in friction between the surface and the powders, until the friction reaches a threshold where the powder aligns with the speed of the rollers. Because there is no slip along the roll surface in the nip zone, the powder must be compressed to the final roll gap dimension. Considering the mass continuity of compacted powder volumes and assuming that, based on empirical evidence, log density is a linear function of log pressure, Johanson (1965) formulated the pressure gradient in the nip region as:

$$\left.\frac{\mathrm{d}\sigma}{\mathrm{d}x}\right|_{nip} = \frac{K\sigma\left(2\cos\theta - 1 - \frac{S}{D}\right)\tan\theta}{\frac{D}{2}\left[\left(1 + \frac{S}{D} - \cos\theta\right)\cos\theta\right]} \quad , \tag{5}$$

where $K$ is the compressibility constant, which is a property of the material. Following that, the nip angle is determined by finding the angle at which the pressure gradients for the slip and non-slip conditions were equal. Therefore, the nip angle can be determined by solving Eqs. (2) and (5) and solving for $\theta = \alpha$:

$$\frac{4\sigma\left(\frac{\pi}{2} - \theta - \nu\right)\tan\delta_E}{\frac{D}{2}\left[1 + \frac{S}{D} - \cos\theta\right]\left[\cot(A - \mu) - \cot(A + \mu)\right]} = \frac{K\sigma\left(2\cos\theta - 1 - \frac{S}{D}\right)\tan\theta}{\frac{D}{2}\left[\left(1 + \frac{S}{D} - \cos\theta\right)\cos\theta\right]} \quad . \tag{6}$$

The resulting SF of the ribbon obtained from the roll compaction process is determined by the maximum pressure applied, or the peak pressure ($P_{max}$), which corresponds to the maximum pressure

exerted on the powder at the minimum roll gap when $\theta = 0$, and can be related to the roller force ( $R_f$), according to:

$$P_{max} = \frac{2R_f}{WDF} \ , \tag{7}$$

where $W$ represents the rolls width, and $F$ is the force factor defined as:

$$F = \int_{\theta=0}^{\theta=\alpha(\delta_E,\phi_W,K)} \left[ \frac{\left(\frac{S}{D}\right)}{\left(1+\frac{S}{D}-\cos\theta\right)\cos\theta} \right]^K \cos\theta \, \mathrm{d}\theta \quad . \tag{8}$$

Eq. (8) implicitly assumes that the contributions of the pressure on the rolls in the slip region and the release region are negligible. Once the peak pressure is known, it can be used to determine the SF (or relative density) that results from the applied pressure of the rolls.

Following the assumption of linear relation between log density and log pressure, the SF $\gamma_R$ of the ribbon can be estimated from the peak pressure as follows:

$$\gamma_R = \gamma_0 P_{max}^{1/K} \ , \tag{9}$$

where $\gamma_0$ is referred to as the pre-consolidation SF, which depends on the powder material. Therefore, $\gamma_0$ and $K$ represent the two materials-dependent parameters of the Johanson model. The pre-consolidation SF $\gamma_0$ corresponds to the SF at a reference pressure of 1 MPa (Moroney et al., 2020). The power-law function expressed in Eq. (9) is referred to as the compression profile of the material under investigation.

In product development, one is interested to know which values of the machine settings (minimum roll gap and roll force) should be employed in an RC to obtain a ribbon of assigned SF. To this purpose, Eq. (9) can be used to return the value of $P_{max}$, from which the required machine settings can be obtained using Eqs. (7) and (8). A preliminary experimental campaign on the RC is required to obtain the powder compression profile, namely, a set of ($\gamma_R$; $P_{max}$) measurements from which the values of $\gamma_0$ and $K$ can be estimated for the powder under investigation. However, this dataset may be difficult or expensive to obtain at the product development stage, due to the lack and cost of materials (especially APIs), as well as to the cost of labor associated to the RC experiments.

## *2.2 Mass correction factor*

In principle, the power law function (Eq. 9) used in the Johanson model may be applied to describe the compaction behavior of powder materials also on a CS, from which experimental data can be collected at a much lower cost. However, significant differences exist in the compression profiles of pharmaceutical blends obtained using rolls or uniaxial dies (Reimer and Kleinebudde, 2019; Reynolds et al., 2010). Namely, the compression profile obtained in a CS for a given powder typically underestimates the pressure required to achieve the same SF using an RC on the same powder. Stated differently, the compression profile parameters ($\gamma_{0CS}$ and $K_{CS}$) estimated from experiments carried out in a CS are typically greater than those ($\gamma_{0\mathrm{RC}}$ and $K_{RC}$) estimated from RC experiments for the same material (Toson et al., 2019). Reynolds et al. (2010) suggested the use of a common material-

dependent compressibility ($K$) value for both pieces of equipment, and to only estimate $\gamma_{0RC}$ to accommodate the differences between the two compactors (Reynolds et al., 2010). However, this approach may become unsatisfactory when the compressibility constant is small. Bi et al. (2014) accounted for the differences by introducing a correction parameter, which they called the mass correction factor, in the derivation of the Johanson model. According to this approach, a relation between the CS pressure ($P_{CS}$) and the peak pressure in the RC exists in the form:

$$P_{CS} = f_0^K P_{max} \ , \tag{10}$$

where $f_0$ represents the mass correction factor. In the derivation of Eq. (10), the mass correction factor is assumed independent of $\theta$. According to Bi et al. (2014), $f_0$ does not depend on the roller force and minimum roll gap, and takes different values (smaller than 1) for three powders mixtures containing the same API in different proportions. So et al. (2021) determined $f_0$ for three pure excipients and concluded that the mass correction factor is material-independent, and its value is $f_0 = 1/1.03 = 0.971$. Validation of these findings on powder mixtures possibly including different APIs have not been reported so far.

# 3 Materials and methods

## *3.1 Materials*

We considered six powder mixtures, consisting of different combinations of four placebo powders (Formulations 1 to 4) and two active compound powders (Formulations 5 and 6). Two different APIs were used, labelled as $API_1$ and $API_2$. Table 1 provides an overview of the materials and compositions of the formulations investigated.

**Table 1.** *List of materials and their compositions (wt.% ) for each of the formulations considered in this study (MCC stands for microcrystalline cellulose).*

| Ingredient | Formulation 1 | Formulation 2 | Formulation 3 | Formulation 4 | Formulation 5 | Formulation 6 |
|---|---|---|---|---|---|---|
| Lactose Anhydrous, SuperTab® AN21 | 70.0 | 50.0 | 30.0 | - | - | 35.5 |
| MCC, Avicel® PH102 | 29.0 | 49.0 | 69.0 | 49.0 | 13.1 | 35.5 |
| MCC, Avicel® PH200 | - | - | - | - | 23.5 | - |
| MgSt | 1.0 | 1.0 | 1.0 | 1.0 | - | 1.0 |
| Mannitol, Peralitol® 200SD | - | - | - | 50.0 | 28.5 | - |
| Sodium starch glycolate, Glycolys® | - | - | - | - | 6.0 | - |

| | | | | | | |
|---|---|---|---|---|---|---|
| Sodium stearyl fumarate, Pruv® | - | - | - | - | 3.0 | - |
| Hydrophilic fumed silica, Aerisol® 200 | - | - | - | - | 0.5 | - |
| Croscarmellose Sodium | - | - | - | - | - | 3.0 |
| $API_1$ | - | - | - | - | 25.4 | - |
| $API_2$ | - | - | - | - | - | 25.0 |

## 3.2 Materials characterization

To use the Johanson model discussed in Section 2.1, $\delta_E$ and $\phi_W$ must be determined for each formulation. These flowability properties were measured using a Brookfield powder flow tester (Brookfield Engineering Laboratories Inc., Middleboro, USA). The effective angle of internal friction was measured using the flow function test in the Brookfield tester, with a maximum consolidation pressure of 6.6 kPa. The wall friction test against stainless steel (smooth 2B finish) was carried out on fresh material at 3 levels of displacement with uniform spacing of 0.01 m, and 7 stress set points up to a maximum stress of 6.6 kPa. The measured values of the powder flow properties are reported in Table 2; in the same table, also the measured values of the true density $\rho_{true}$ of each formulation are reported (to be discussed in Section 3.5).

**Table 2.** *Properties measured for each formulation.*

| **Material** | $\phi_w$ (°) | $\delta_E$ (°) | $\rho_{true}$ (g/cm$^3$) |
|---|---|---|---|
| Formulation 1 | 12.5 | 38.0 | 1.554 |
| Formulation 2 | 9.0 | 37.5 | 1.563 |
| Formulation 3 | 11.0 | 44.0 | 1.572 |
| Formulation 4 | 16.0 | 51.0 | 1.547 |
| Formulation 5 | 39.5 | 44.2 | 1.470 |
| Formulation 6 | 23.2 | 46.8 | 1.530 |

## 3.3 Roller compactor experiments

The RC experimental campaign was performed using the Gerties Mini-Pactor® (Gerteis Machinen + Process Engineering AG, Jona, Switzerland). The knurled rolls had a diameter of 250 mm and a width of 25 mm. The rim roll sealing system was installed in order to prevent materials leaking during the roll compaction process. The RC was operated in gap-controlled mode, wherein the roll force and roll gap were kept constant by regulating the input of feed material via the screw feeder. We conducted multiple runs with different machine settings to examine the behavior of compacted powder under varying levels of applied pressure. The rotational speed of the roll was maintained at a constant value of 2 rpm, while the specific roll force applied to the roll gap were adjusted accordingly for each experimental run. The summary of the entire RC experimental campaign is reported in Table 3. Note that performing an experimental campaign at four different conditions (i.e., four runs) for a given formulation requires at least 2.5 kg of material, which is a considerable amount at the development stage, especially if APIs are to be used.

**Table 3.** *Roll compaction experiments conducted for each material.*

| Material | Specific roll force (kN/cm) | Roll gap (mm) | No. of runs |
|---|---|---|---|
| Formulation 1 | 3.0 | 2 | 1 |
| | 6.0 | 2 | 1 |
| | 9.0 | 2 | 1 |
| | 12.0 | 2 | 1 |
| | 4.2 | 4 | 1 |
| Formulation 2 | 3.0 | 2 | 1 |
| | 6.0 | 2 | 1 |
| | 9.0 | 2 | 1 |
| | 12.0 | 2 | 1 |
| Formulation 3 | 4.2 | 4 | 1 |
| Formulation 4 | 8.5 | 4 | 1 |
| | 3.0 | 4 | 1 |
| | 6.0 | 4 | 1 |
| Formulation 5 | 4.0 | 2 | 2 |
| | 6.0 | 2 | 11 |
| | 8.0 | 2 | 8 |
| | 5.0 | 3 | 2 |

| | | | |
|---|---|---|---|
| | 7.5 | 3 | 2 |
| | 10.0 | 3 | 2 |
| | 14.0 | 3 | 2 |
| Formulation 6 | 3.5 | 2 | 1 |
| | 5.5 | 2 | 7 |
| | 10.0 | 2 | 1 |
| | 6.5 | 3 | 1 |

## 3.4 Compactor simulator experiments

The CS experimental campaign was performed using the Phoenix® CS (Phoenix Calibration and

Services Ltd, Brierley Hill, UK) equipped with round flat faced punches with tooling diameters of 10 mm. In every trial, a mechanized procedure was employed to load the CS die with a predetermined quantity of the powder blend. The pressure was exerted by two punches moving in opposite directions with a sinusoidal displacement profile, according to the model proposed by Zinchuk et al. (2004). The experimental campaigns consisted of 35 to 40 experiments for each material, with the applied pressure ranging from 20 to 250 MPa. Approximately 250 mg of powder mixture is required for a single test with this setup. Therefore, for a full experimental campaign on the CS, ~10 grams of powder are required, which is considerably less compared to the amount used on the RC.

## 3.5 Solid fraction experimental determination

SFs were calculated for each ribbon from the measured values of the envelope density $\rho_{env}$ and mixture true density $\rho_{true}$ as:

$$\gamma_R = \frac{\rho_{env}}{\rho_{true}} \quad . \tag{11}$$

For each RC experimental run, three rectangular samples measuring 25 by 10 mm were collected from the produced ribbons to assess the envelope density. Three independent samples were collected from different segments of the ribbon to address the potential variability of SF across its width (Mazor et al., 2016). The envelope density of each sample was measured using a powder pycnometer Geopyc® either 1360 or 1365 (Micrometrics, USA). The measuring chamber of the powder pycnometer had a diameter of 25.4 mm, the consolidation force was set at 51 N, and the conversion factor was 0.5153 cm$^3$/mm. A mean value of $\rho_{env}$ from triplicate envelope density measurements was calculated for use in (11). After the powder mixes were compacted using the CS, the samples were ejected from the die by the lower punch. The GeoPyc® 1360 powder pycnometer was used to measure the envelope density of the produced CS ribblets, following the previously stated procedure.

The true densities of all the components in the formulation were measured using a helium pycnometer (Accupyc® 1330, Micrometrics, USA). The true density of the blend was then calculated as the mass fraction weighted average of the true densities of the constituent components. The resulting $\rho_{true}$ for all the formulations are reported in Table 2.

### 3.6 Johanson model parameter estimation

For a given formulation, calibration of the Johanson model parameters $\gamma_0$ and $K$ in Eq. (9) was carried out using a maximum-likelihood estimation approach; the approach was the same regardless of whether the datasets were obtained from an RC or a CS (with $P_{CS}$ being used instead of $P_{max}$). Namely, the $\gamma_0$ and $K$ estimates were determined in such a way as to minimize the following objective function (Bard, 1974):

$$-\ell = +\frac{N}{2}\ln 2\pi\sigma^2 + \frac{1}{2\sigma^2}\sum_{i=1}^{N}(\gamma_{R,i}^{exp} - \gamma_{R,i}^{calc})^2 \quad , \tag{12}$$

where: $\ell$ is the log-likelihood function; $\gamma_{R,i}^{exp}$ is the experimental ribbon SF for experimental point $i$; $\gamma_{R,i}^{calc}$ is the calculated ribbon SF for experimental point $i$; $N$ is the overall number of experimental points available for the given formulation; and $\sigma^2$ is the variance of measurement errors, which are assumed to be normally distributed (Bard, 1974). The procedure was performed using the `fminunc` function in Matlab® R2023a. Upon estimation of the model parameters, their associated confidence intervals were also evaluated from the parameter variance-covariance matrix, as obtained by inversion of the Hessian matrix (Greene, 2011).

## 4 Proposed transfer methodology

In this Section, we propose a methodology to establish a relation between the compression profile of a given material on a CS and the compression profile of the same material on an RC. We refer to this as to a (data) transfer methodology; from a general perspective, this type of activity is also referred to as "transfer learning" in the literature (Zhuang et al., 2021).

The proposed transfer methodology is based on the mass correction factor approach (Bi et al., 2014). The flow chart in Figure 2 illustrates the framework for *i*) design and calibration, *ii*) validation, and *iii*) usage of the transfer methodology. This study focuses on steps *i*) and *ii*). Once the methodology is validated, step *iii*) can be used to deploy the transfer methodology industrially by incorporating into the operating procedures that are in place for new formulations.

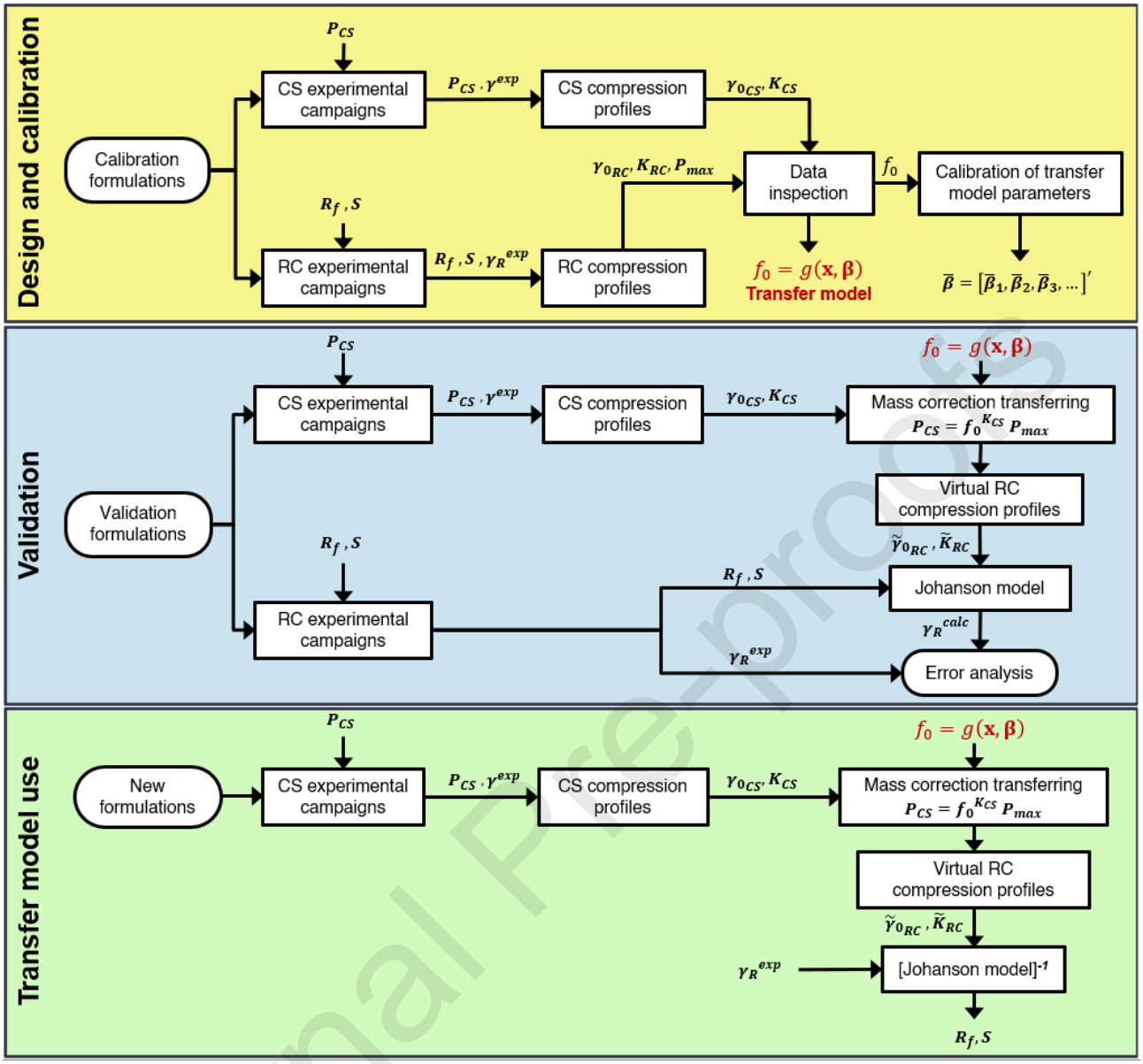


**Figure 2.** *Flow chart of the design/calibration, validation, and usage steps of the proposed CS-to-RC transfer methodology based on the mass correction factor.*

## 4.1 Design and calibration of the transfer model

Design and calibration of the transfer model was accomplished using datasets from Formulations 1, 2, 3 and 4, which do not include APIs (see Table 3). This was done on purpose, because it is known that the presence of an API can significantly alter the flowability and compressibility properties of a powder blend (Megarry et al., 2019). Therefore, by using materials that do not contain APIs, we make the transfer model validation step more challenging. Next, we detail the procedure followed for each formulation (upper flow chart in Figure 2).

Using experimental data obtained from experimental campaigns conducted on the CS and the RC, the relevant compaction parameters ($\gamma_{0CS}$ and $K_{CS}$ for the CS, and $\gamma_{0RC}$ and $K_{RC}$ for the RC) were obtained as discussed in Section 3.6. The compression profiles were then compared to assess the mismatch between the estimated $P_{max}$ resulting from the RC experimental data, and the pressure $P_{CS}$ required in the CS to obtain the same SF. The point values $f_{0,i}$ of the mass correction factor (i.e., the

values of $f_0$ required for matching the pressures of both machines at each value of the SF for each RC experimental point $i$) were determined by inverting Eq. (10), namely:

$$f_{0,i} = \left(\frac{P_{CS,i}}{P_{max,i}}\right)^{\frac{1}{K}} \quad , \tag{13}$$

with $K = K_{CS}$. The point values of $f_0$ for all formulations were investigated to identify possible relationships of the mass correction factor with respect to the RC operating parameters and/or material parameters (Bi et al., 2014). In this step, we sought to find a function $g(\mathrm{x},\beta)$ (called the transfer model) able to return a suitable value for $f_0$ for a given (sub)set x of RC operating parameters and/or materials properties, where β are the transfer model parameters; stated differently, we looked for $f_0 = g(\mathrm{x},\beta)$, where the functional form $g(\cdot)$, as well as the elements of x and the values $\overline{\beta}$ of the parameters, were unknown. Once $g(\mathrm{x},\beta)$ was found, estimation of the parameter set (together with the confidence interval of each parameter) concluded the calibration step.

## *4.2 Validation of the transfer model*

The aim of the validation is to show how effectively the transfer model allows a compression profile obtained in a CS to be transferred to a compression profile valid for an RC for powder mixtures *not* used in the calibration step. To this purpose, data from Formulations 5 and 6 (which include APIs) were used. Next, we discuss the validation procedure for one given validation formulation (center flow chart in Figure 2).

First, the values of $\gamma_{0CS}$ and $K_{CS}$ were estimated from CS experiments on the investigated formulation. Then, using these values and the transfer model, virtual Johanson model parameters for the RC (namely, $\tilde{\gamma}_{0RC}$ and $\tilde{K}_{RC}$) were derived. Here, the attribute "virtual" denotes a Johanson model built for the RC using experimental data coming from the CS jointly with the mass correction factor $f_0$ calculated by means of the transfer model $g(\mathrm{x},\beta)$. As a result, the Johanson model describing the behavior of this material on the RC could be established without the need for an experimental campaign on the RC itself. By using $\tilde{\gamma}_{0RC}$ and $\tilde{K}_{RC}$, the Johanson model was then solved using the machine setting combinations (namely, $R_f$ and $S$) employed during the RC experimental campaign, thus determining the calculated values $\gamma_{R,i}^{calc}$ of the ribbon SF at those operating conditions (experimental point $i$). These values were finally compared to the relevant experimental values of $\gamma_{R,i}^{exp}$ obtained using the same combinations of machine settings.

To evaluate the transfer results, the mean absolute error (MAE) and the mean relative error (MRE) were used as performance indicators:

$$\mathrm{MAE} = \frac{1}{N}\sum_{i=1}^{N} |y_i^{calc} - y_i^{exp}| \quad , \tag{14}$$

$$\mathrm{MRE} = \frac{1}{N}\sum_{i=1}^{N} \frac{|y_i^{calc} - y_i^{exp}|}{y_i^{exp}} \quad , \tag{15}$$

where $y = \gamma_R$.

### 4.3 Usage of the transfer methodology

The investigation of a new powder mixture involves conducting an experimental campaign *solely on the CS*, as illustrated in the lower flow chart of Figure 2. The resulting experimental data can then be used to estimate the values of $\gamma_{0CS}$ and $K_{CS}$, which can be used jointly with the transfer model to obtain the virtual Johanson model parameter values, $\tilde{\gamma}_{0RC}$ and $\tilde{K}_{RC}$. These values enable using the Johanson model, in its inverse form, to determine the RC machine settings ${R_f}^{calc}$ and $S^{calc}$ that are required to obtain the desired ribbon SF, $\gamma_R^{des}$. Furthermore, knowing $\tilde{\gamma}_{0RC}$ and $\tilde{K}_{RC}$ makes it possible to explore the design space of the RC for the given formulation, and therefore to analyze how the SF is affected by different combinations of machine parameters.

## 5 Results and discussion

### 5.1 Compression profiles for the calibration and validation formulations

Estimation of the Johanson model parameters for all formulations was obtained as outlined in Section 3.6. With respect to the RC datasets, after obtaining the values of $\gamma_{0\mathrm{RC}}$ and $K_{RC}$ for a given formulation, the peak pressures $P_{max}$ were calculated for each experimental combination of roll gap and specific roll force. Table 4 presents the estimated values of the Johanson model parameters, along with their 95% confidence intervals and with the model $R^2$ values.

**Table 4.** *Compaction parameters, $\gamma_0$ and K, and relevant 95% confidence intervals estimated from experimental campaigns on the C and RC for calibration and validation formulations.*

| Material | Roller compactor | | | Compactor simulator | | |
|---|---|---|---|---|---|---|
| | $\gamma_{0\mathrm{RC}}$ (-) | $K_{RC}$ (-) | $R^2$ | $\gamma_{0\mathrm{CS}}$ (-) | $K_{CS}$ (-) | $R^2$ |
| Formulation 1 | 0.345 ± 0.04 | 6.054 ± 1.05 | 0.93 | 0.422 ± 0.02 | 7.449 ± 0.65 | 0.96 |
| Formulation 2 | 0.242 ± 0.02 | 4.199 ± 0.44 | 0.95 | 0.358 ± 0.02 | 5.973 ± 0.46 | 0.98 |
| Formulation 3 | 0.198 ± 0.02 | 3.475 ± 0.31 | 0.98 | 0.326 ± 0.02 | 5.340 ± 0.40 | 0.98 |
| Formulation 4 | 0.233 ± 0.02 | 4.120 ± 0.42 | 0.97 | 0.336 ± 0.02 | 5.611 ± 0.45 | 0.98 |
| Formulation 5 | 0.267 ± 0.03 | 4.599 ± 0.55 | 0.83 | 0.363 ± 0.02 | 6.090 ± 0.62 | 0.98 |
| Formulation 6 | 0.343 ± 0.10 | 6.223 ± 2.71 | 0.49 | 0.389 ± 0.02 | 6.477 ± 0.58 | 0.96 |

The values of the compression parameters derived from CS data are also reported in Table 4. Expectedly, increasing the composition of MCC (Formulations 1 to 3) results in decreased values of both $\gamma_0$ and $K$. By comparing placebo Formulations 2 and 4, which exhibit comparable compaction behavior, we infer that lactose (Formulation 1) and mannitol (Formulation 4) have a similar impact on the compaction behavior. Finally, note that the RC data for Formulation 6 return wide confidence intervals for the Johanson model parameters, and a relatively small value of $R^2$. This suggests that the available SF measurements for this formulation are affected by strong variability, probably due to fragile behavior of the ribbon samples.

For each formulation, Figure 3 shows the experimental data obtained in the RC and CS, together with the relevant compression profiles obtained by fitting the experimental data by means of the Johanson model.

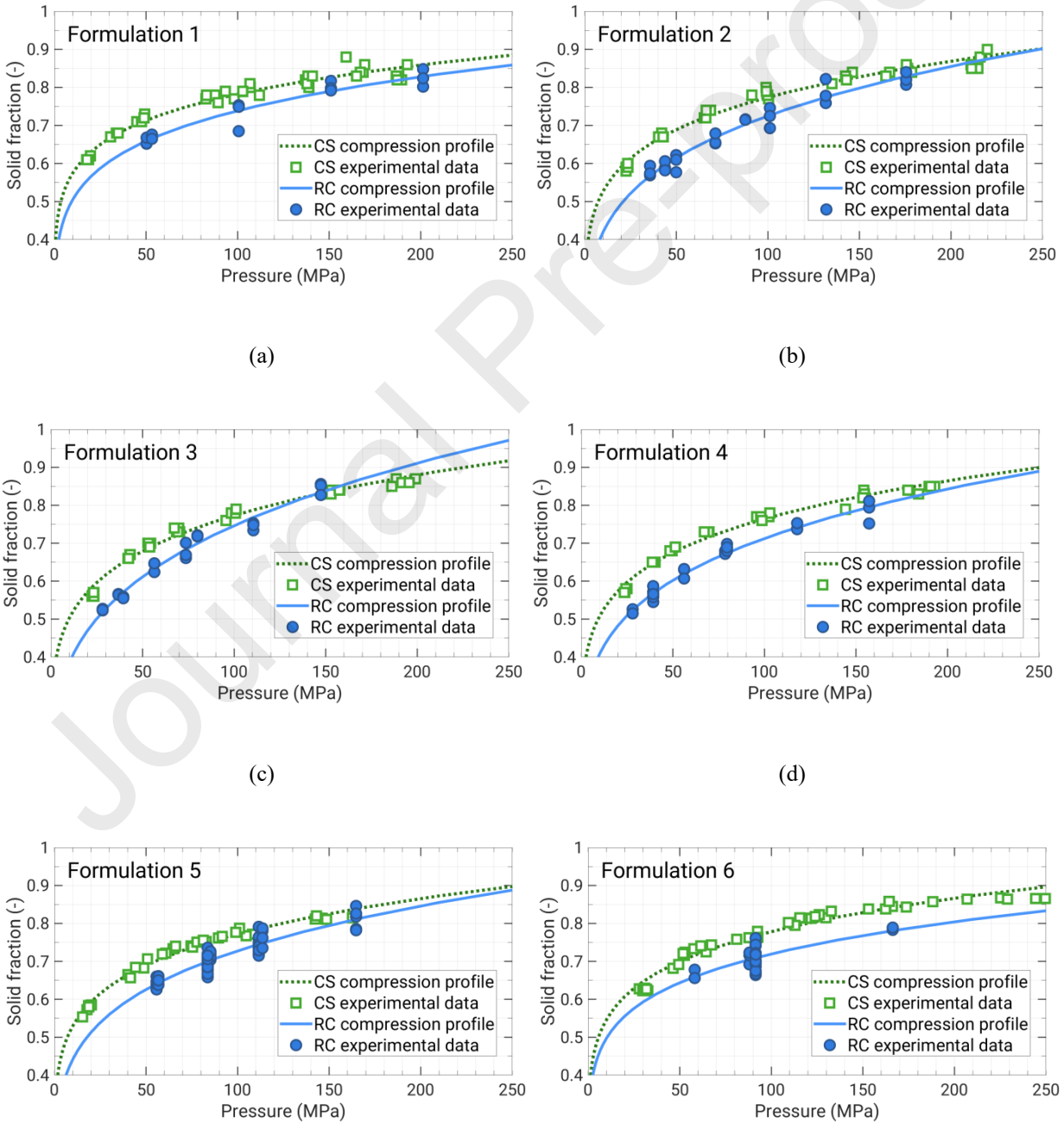


(a) (b)

(c) (d)

(e) (f)

**Figure 3.** *Comparison between RC compression profiles and CS compression profiles for: (a) Formulation 1, (b) Formulation 2, (c) Formulation 3, (d) Formulation 4, (e) Formulation 5, (f) Formulation 6. The compression profiles have been obtained by fitting of the related experimental data.*

For all formulations (with the exception of Formulation 3 at large $P_{max}$ values), the compression profile obtained from CS experiments underestimates the pressure required to attain the same SF in an RC. This confirms that a Johanson model calibrated using parameters derived from CS data is unsuitable for direct characterization of roll compaction operations of pharmaceutical powders, consistently with the outcomes of Bi et al. (2014), Reynolds et al. (2010), So et al. (2021), and Toson et al. (2019).

## 5.2 Design and calibration of the transfer model

Figure 4 illustrates how the mass correction factor, calculated for all the RC experimental points available for the calibration mixtures, changes with the RC peak pressure. We notice that, for a given formulation, $f_0$ is not constant, but changes with $P_{max}$, with ln $(f_0)$ increasing roughly linearly with ln $(P_{max})$. This differs from the study of So et al. (2021), who used a constant value of $f_0$ for any combination of machine settings, i.e., for any peak pressure. The increasing trend of $f_0$ with $P_{max}$ is physically reasonable. In fact, $f_0$ represents the fraction of material that is delivered at the minimum roll gap, and is affected by the particle velocity gradients. As the pressure exerted by the rollers increases, the powder particles become less loose in the nip region, resulting in a greater quantity of powder being conveyed to the minimal roll gap. On the other hand, no particular trends of $f_0$ were observed with respect to other operating parameters of the RC or to the powder flow properties.

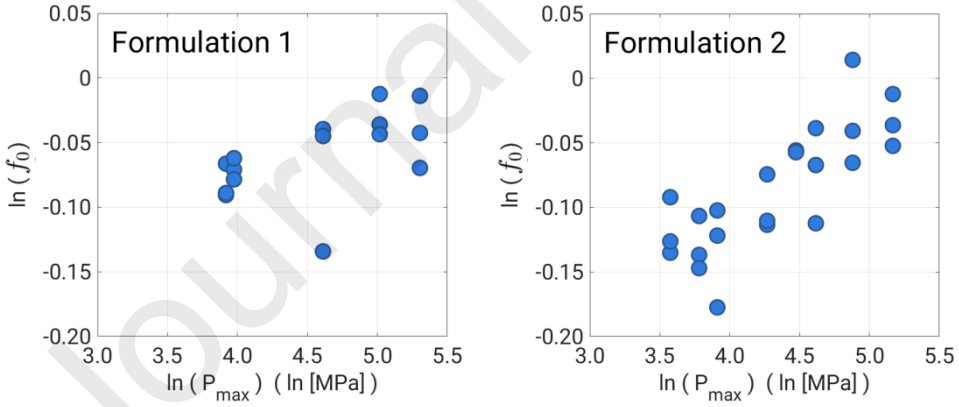


(a) (b)

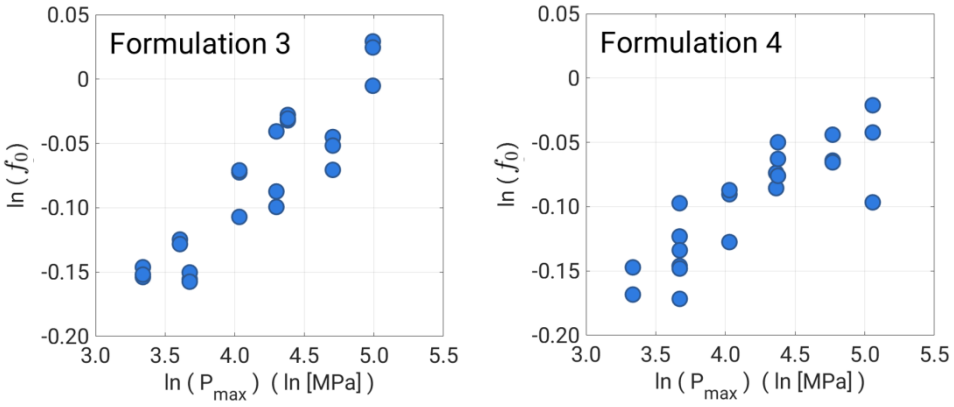


(c) (d)

**Figure 4.** *Mass correction factor versus peak pressure in the RC, calculated from all RC calibration data for: (a) Formulation 1; (b) Formulation 2, (c) Formulation 3, (d) Formulation 4.*

The transfer model was therefore designed as:

$$\ln f_0 = \beta_1 + \beta_2 \ln P_{max} \quad . \tag{16}$$

Using the notation introduced in Section 4.1 and in Figure 2, the transfer model can be written as:

$$f_0 = g(\mathrm{x},\beta) = e^{\beta_1} e^{(\beta_2 \ln P_{max})} \tag{17}$$
$$= e^{\beta_1} \cdot P_{max}^{\beta_2} \quad ,$$

where $\mathrm{x} = [P_{max}]$, and $\beta = [\beta_1; \beta_2]^{\mathrm{T}}$. Notice that the transfer model is a generalized equation, meaning that it is mixture-independent, which is a considerable advantage from a product development perspective. The values of $\beta_1$ and $\beta_2$ were determined in such a way as to minimize the horizontal distance between the compression profiles obtained in the CS and RC at the SFs obtained from the RC experiments. As a result, the following values were obtained: $\overline{\beta}_1 = -0.248 \pm 0.068$ and $\overline{\beta}_2 = 0.042 \pm 0.017$. This turns the transfer model into:

$$f_0 = 0.7804\, P_{max}^{0.042} \quad . \tag{18}$$

Figure 5 illustrates how the mass correction factor changes with the peak pressure for all available calibration points and according to the proposed transfer model (Eq. 18). The prediction uncertainty on $f_0$ (with a confidence level of 95%) was determined using multivariate parameter sampling based on the parameter covariance matrix (Tong, 1990). The transfer model was benchmarked against a model in which a single, optimal value of $f_0$ was used at all pressures. This value was estimated to be $\overline{f}_0 = 0.958 \pm 0.008$; interestingly, it is close to (yet different from) the value $\overline{f}_0 = 0.971$ obtained by So et al. (2021) for three excipients that are different from the powders considered in this study (So et al., 2021); information about the uncertainty of the value found by So et al. (2021) was not reported in the original paper.

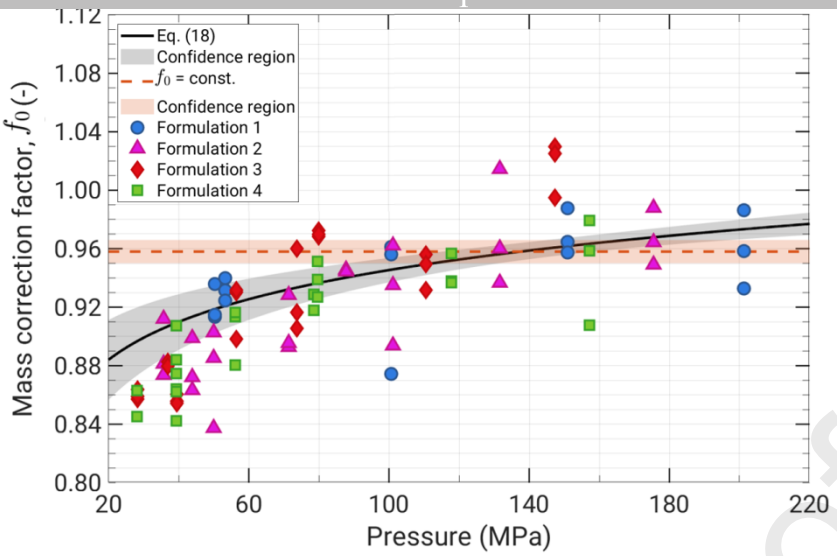


**Figure 5.** *Calibration results. Mass correction factor $f_0$ as a function of the peak pressure $P_{max}$ for three cases: i) as calculated for all calibration points (symbols); ii) as predicted by the proposed transfer model (18) (solid black line), with related 95% confidence interval; and iii) as a constant optimal value of 0.958 (broken red line), with related 95% confidence interval.*

Figure 5 clarifies that when pressure exceeds 100 MPa, the responses of the two models are not very different. However, at lower pressures the proposed transfer model (Eq. 18) returns values of $f_0$ that are much closer to those that would imply perfect reproduction of the experimental RC compression profile.

To quantify the performance of the transfer models in calibration, each experimental point obtained in the RC (circles in Figure 3) was transferred onto the compression profiles obtained from experiments on the CS (dotted lines in Figure 3). Namely, for the value of SF obtained in the RC at a given peak pressure, the relevant CS pressure was calculated by determining $f_0$ through (Eq. 18) or $\overline{f}_0 = 0.958$, and then $P_{CS}$ through (Eq. 10). This calculated value was compared to the one obtained from the CS compression profile at the same value of SF. The results, in terms of MAE and MRE, are reported in Table 5. The results demonstrate that using the proposed model consistently yields lower MAEs and MREs in calibration for all formulations, suggesting that adopting a variable value of $f_0$ significantly improves data transfer.

**Table 5.** *Calibration results. Mean absolute and relative errors on CS pressure between the projection of the RC experimental data on the CS compression profile and the experimental data using two different models to calculate $f_0$.*

| **Material** | $f_0 = 0.7804\ P_{max}^{0.042}$ | | $f_0 = \text{const.} = 0.958$ | |
|---|---|---|---|---|
| | **MAE (MPa)** | **MRE (%)** | **MAE (MPa)** | **MRE (%)** |
| Formulation 1 | 11.2 | 15.1 | 12.6 | 22.6 |
| Formulation 2 | 8.3 | 18.0 | 13.1 | 37.1 |

| | | | | |
|---|---|---|---|---|
| Formulation 3 | 10.0 | 18.6 | 13.3 | 37.7 |
| Formulation 4 | 5.9 | 17.6 | 11.2 | 41.9 |

## 5.3 Validation of the transfer model

Following Eq. (9), the compression profile obtained in a CS can be expressed as:

$$\gamma = \gamma_{0CS} P_{CS}^{1/K_{CS}} \quad . \tag{18}$$

Substitution of Eq. (10) into Eq. (18) gives:

$$\gamma = \gamma_{0CS} \left(f_0^{K_{CS}} P_{max}\right)^{1/K_{CS}} \quad . \tag{19}$$

Then, substitution of Eq. (17) into Eq. (19) gives:

$$\gamma = \gamma_{0CS} \left[ (e^{\beta_1} P_{max}{}^{\beta_2})^{K_{CS}} P_{max} \right]^{1/K_{CS}} \quad . \tag{20}$$

Upon algebraic manipulation, Eq. (20) can be reformulated as:

$$\gamma = \gamma_{0CS} e^{\beta_1} P_{max}{}^{\frac{\beta_2 K_{CS}+1}{K_{CS}}} \quad . \tag{21}$$

The above power-law function represents the compression profile for the RC. Comparison of Eq. (16) with Eq. (9) allows one to formulate the virtual compression profile in an RC as the one obtained by transfer of the compression profile obtained in a CS:

$$\tilde{\gamma} = \tilde{\gamma}_{0RC} P_{max}^{1/\tilde{K}_{RC}} \quad , \tag{22}$$

where $\tilde{\gamma}$ is the ribbon SF as transferred from the CS, and the virtual Johanson model parameters $\tilde{\gamma}_{0RC}$ and $\tilde{K}_{RC}$ are defined as:

$$\tilde{\gamma}_{0RC} = \gamma_{0CS} e^{\beta_1} = 0.780\, \gamma_{0CS} < \gamma_{0CS} \quad , \tag{23}$$

$$\tilde{K}_{RC} = \frac{K_{CS}}{\beta_2 K_{CS} + 1} = \frac{K_{CS}}{0.042 K_{CS} + 1} < K_{CS} \quad . \tag{24}$$

The proposed transfer model is therefore able to provide explicit algebraic equations to transfer both the pre-consolidation SF and the compressibility values obtained from CS experiments to the values valid for an RC. From this, a virtual RC compression profile (i.e., one obtained solely from experiments carried out in a CS) can be obtained straightforwardly.

Figure 6 proposes a visual comparison between the compression profiles obtained in the RC and the virtual ones obtained by transfer learning according to the proposed transfer model or to $f_0 = \text{const.}$ For Formulation 5, the proposed transfer model enables almost perfect overlap between the virtual compression profile and the true one; the overlap is still good (especially at medium-to-low pressures) for Formulation 6, for which the available experimental points are fewer and with greater uncertainty. Conversely, a simpler model ($f_0 = \text{const.}$) is less effective in data transfer.

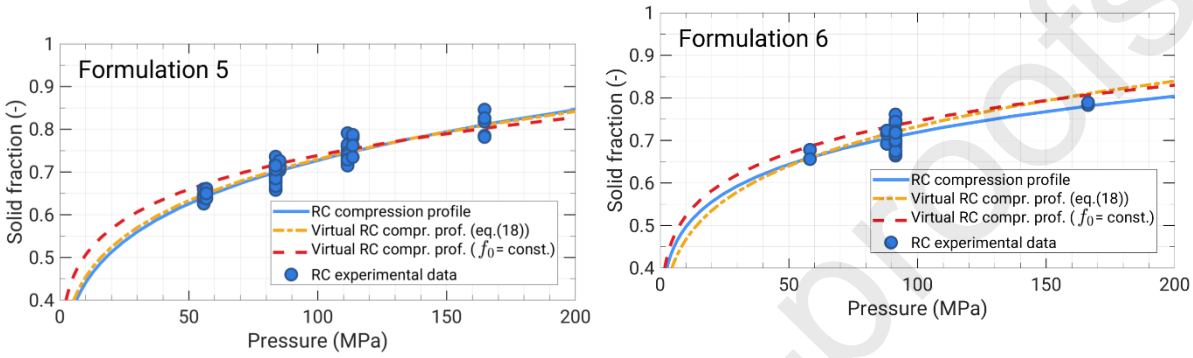


(a) (b)

**Figure 6.** *Validation results. Comparison between the compression profile obtained by regression of RC experimental data and the virtual RC compression profile obtained by transfer of CS data using the proposed model (17) and $f_0 = 0.958$ for: (a) Formulation 5 and (b) Formulation 6.*

Table 6 summarizes the validation results in terms of model parameters and SF estimations for all operating conditions for which an experimental value of the SF is available in the RC.

**Table 6.** *Validation results. The Johanson model parameters are obtained by regression of RC data, by regression of CS data transferred using (18), and by regression of CS data transferred using $f_0 = 0.958$. The errors refer to SFs.*

| **Material** | **Compression profile** | **Johanson model parameter** | | **MAE** | **MRE (%)** | $R^2$ |
|---|---|---|---|---|---|---|
| | | $\gamma_{0RC}$ or $\tilde{\gamma}_{0RC}$ | $K_{RC}$ or $\tilde{K}_{RC}$ | | | |

| | | | | | | |
|---|---|---|---|---|---|---|
| | from RC data | 0.267 | 4.599 | 0.016 | 2.2 | 0.83 |
| Formulation 5 | by transfer from CS data using (18) | 0.283 | 4.857 | 0.017 | 2.4 | 0.80 |
| | by transfer from CS data using $f_0 = 0.958$ | 0.347 | 6.090 | 0.036 | 5.2 | 0.24 |
| | from RC data | 0.343 | 6.223 | 0.019 | 2.6 | 0.49 |
| Formulation 6 | by transfer from CS data using (18) | 0.298 | 5.100 | 0.020 | 2.8 | 0.47 |
| | by transfer from CS data using $f_0 = 0.958$ | 0.366 | 6.477 | 0.032 | 4.6 | -0.27 |

For Formulation 5, the Johanson model parameters obtained by regression of virtual data (i.e., of CS data transferred using the proposed transfer model) closely match the parameter values obtained by direct experimentation in a RC, and both MAE and MRE are comparable to those obtained by direct experimentation; on the other hand, using a constant value of $f_0$ is unable to provide effective data transfer, leading to almost double values of MAE and MRE, and poor $R^2$. For Formulation 6, the SF values returned by applying the proposed transfer methodology from CS data closely match those provided by direct experimentation on an RC (almost identical values of MAE and MRE); instead, the performance of a transfer model that uses a constant value of $f_0$ is poor.

Having the proposed methodology been validated, one can use it to investigate the design space of the RC for any new developed formulation, as discussed in Section 4.3 and illustrated in the lower flow chart of Figure 2.

## 6 Conclusions

This study has analyzed the compaction behavior of pharmaceutical powders to be used in tablet manufacturing. The main issue investigated was the possibility of deriving the compression profile of a powder mixture in a roller compactor (RC) from the compression profile obtained for the same in a compactor simulator (CS). We based our investigation on the well-known Johanson model, which describes roller compaction, and on the mass corrector factor theory, which corrects the Johanson model when the compression profile of a powder is obtained from CS experiments.

We analyzed the behavior of six powder mixtures, two of which including active pharmaceutical ingredients, when compacted in an RC or in a CS. The experimental data confirmed that, for a given mixture, the RC and CS compression profiles are different. We found that accurate transfer of a CS compression profile to an RC compression profile requires the mass correction factor to be expressed as a function of the pressure, regardless of the powder being compacted. We developed a simple log-

log linear correlation (which we called the transfer model) between the mass correction factor and pressure in the RC, which allows one to calculate the Johanson model parameters for an RC once the parameters in a CS are known. We showed that the RC compression profiles predicted by the proposed transfer learning methodology accurately reproduce those obtained by direct experimentation on an RC.

Our study improves on previous work on the same topic in the following respects: *i*) the number of powder mixtures investigated is larger; *ii*) we do not consider single-component powders, and we consider the presence of active pharmaceutical ingredients in some of the powders; *iii*) we show that using a variable mass transfer coefficient significantly improves the prediction of the RC compression profile over the case where the mass correction factor is constant; *iv*) we provide a straightforward equation to calculate the mass correction factor for any powder; *iv*) we provide calibration *and* validation results.

We believe that industrial deployment of the proposed transfer methodology has the potential to result in significant savings in resources, time, and cost.

## List of symbols

| | |
|---|---|
| $D$ | Roll diameter |
| $F$ | Force factor |
| $f_0$ | Mass correction factor |
| $g(\mathrm{x},\beta)$ | Transfer model |
| $i$ | Generic experimental data |
| $K$ | Compressibility constant |
| $K_{CS}$ | Compressibility constant estimated from compactor simulator experimental data |
| $K_{RC}$ | Compressibility constant estimated from roller compactor experimental data |
| $\tilde{K}_{RC}$ | Compressibility constant estimated using the mass correction factor transfer methodology |
| $\ell$ | Log-likelihood function |
| $N$ | Overall number of experimental data |
| $P_{CS}$ | Maximum pressure applied by the compactor simulator |
| $P_{max}$ | Maximum roller surface pressure at the minimum roll gap |
| $R_f$ | Total roll force |
| $S$ | Roll gap |
| $W$ | Roll width |
| $\mathbf{x}$ | Vector of roller compactor operating parameters and material properties |

*Greek letters*

| | |
|---|---|
| $\alpha$ | Nip angle |
| $\boldsymbol{\beta}$ | Vector of transfer model parameters |
| $\gamma$ | Solid fraction |
| $\gamma_0$ | Preconsolidation relative density |
| $\gamma_{0CS}$ | Preconsolidation relative density estimated from compactor simulator experimental data |
| $\tilde{\gamma}_{0RC}$ | Preconsolidation relative density estimated using the mass correction factor transfer methodology |
| $\gamma_{0RC}$ | Preconsolidation relative density estimated from roller compactor experimental data |
| $\gamma_R$ | Ribbon solid fraction |
| $\gamma^{exp}$ | Experimental solid fraction |
| $\gamma_R^{exp}$ | Experimental ribbon solid fraction |
| $\gamma_R^{calc}$ | Calculated ribbon solid fraction |
| $\delta_E$ | Effective angle of internal friction |
| $\theta$ | Angular roll position |
| $\mu$ | Friction coefficient |
| $\nu$ | Acute angle between major principal axis and tangent to roll surface |
| $\rho_{env}$ | Envelope density |
| $\rho_{true}$ | True density |
| $\phi_W$ | Angle of wall friction |

*Acronyms*

| | |
|---|---|
| API | Active pharmaceutical ingredient |
| CS | Compactor simulator |
| MAE | Mean absolute error |
| MCC | Microcrystalline cellulose |
| MgSt | Magnesium stearate |
| MRE | Mean relative error |
| RC | Roller compactor |
| SF | Solid fraction |

## CRediT author statement

Luca Beccaro: Conceptualization; Methodology; Software; Validation; Formal analysis; Data curation; Writing – original draft; Visualization

Pierantonio Facco: Conceptualization; Methodology; Formal analysis; Writing – review & editing

Ranjit M. Dhenge: Investigation; Resources; Writing – review & editing

Marv J. Khala: Investigation; Resources

Francesca Cenci: Writing – review & editing

Fabrizio Bezzo: Conceptualization; Methodology; Formal analysis; Writing – review & editing

Massimiliano Barolo: Conceptualization; Methodology; Formal analysis; Writing – review & editing; Supervision; Project administration; Funding acquisition

## Declaration of competing interest

R.M. Dhenge and F. Cenci are employees of GSK and may hold share options and/or shares in GSK. M.J. Khala was an employee of GSK at the time this study was carried out. The authors declare no other competing conflicts of interest.

## Data availability

The data used in this study are made available in the Supplementary material.

## Supplementary material

The supplementary material contains all the data that were used to carry out this study.

## References


Adeyeye, M. C., 2000. Roller compaction and milling pharmaceutical unit processes: Part I. American Pharm. Rev., 3, 37–42. https://doi.org/10.1208/s12249-008-9088-y

Amini, H., Akseli, I., 2020. A first principle model for simulating the ribbon solid fraction during pharmaceutical roller compaction process. Powder Technology 368, 32–44. https://doi.org/10.1016/j.powtec.2020.04.022

Bano, G., Dhenge, R.M., Diab, S., Goodwin, D.J., Gorringe, L., Ahmed, M., Elkes, R., Zomer, S., 2022. Streamlining the development of an industrial dry granulation process for an immediate release tablet with systems modelling. Chem. Eng. Res. Des. 178, 421–437. https://doi.org/10.1016/j.cherd.2021.12.033

Bard, Y., 1974. Nonlinear Parameter Estimation. New York ; London : Academic press.

Bi, M., Alvarez-Nunez, F., Alvarez, F., 2014. Evaluating and Modifying Johanson's Rolling Model to Improve its Predictability. J. Pharm. Sci. 103, 2062–2071. https://doi.org/10.1002/jps.24012

Dec, R.T., Zavaliangos, A., Cunningham, J.C., 2003. Comparison of various modeling methods for analysis of powder compaction in roller press. Powder Technol. 130, 265–271. https://doi.org/10.1016/S0032-5910(02)00203-6

Desai, P.M., Bhugra, C., Chowdhury, A., Melkeri, Y., Patel, H., Lam, S., Hayden, T., 2024. Implementation of mechanistic modeling and global sensitivity analysis (GSA) for design, optimization, and scale-up of a roller compaction process. Int. J. Pharm. 658, 124201. https://doi.org/10.1016/j.ijpharm.2024.124201

Farber, L., Hapgood, K.P., Michaels, J.N., Fu, X.-Y., Meyer, R., Johnson, M.-A., Li, F., 2008. Unified compaction curve model for tensile strength of tablets made by roller compaction and direct compression. Int. J. Pharm. 346, 17–24. https://doi.org/10.1016/j.ijpharm.2007.06.022

Gavi, E., Reynolds, G.K., 2014. System model of a tablet manufacturing process. Comput. Chem. Eng. 71, 130–140. https://doi.org/10.1016/j.compchemeng.2014.07.026

Greene, W.H., 2011. Econometric Analysis, 7th edition. ed. Pearson, Boston Munich.

Guigon, P., Simon, O., Saleh, K., Bindhumadhavan, G., J. Adams, M., Seville, J.P.K., 2007. Chapter 5 Roll pressing, in: Salman, A.D., Hounslow, M.J., Seville, J. P. K. (Eds.), Handbook of Powder Technology, Granulation. Elsevier Science B.V., pp. 255–288. https://doi.org/10.1016/S0167-3785(07)80040-6

Hassan, L., Jensen, R., Megarry, A., Blaabjerg, L.I., 2023. Simulation of roller compaction by combination of a compaction simulator and oscillating mill – A material sparing approach. Int. J. Pharm. 644, 123281. https://doi.org/10.1016/j.ijpharm.2023.123281

Jenike, A.W., Shield, R.T., 1959. On the Plastic Flow of Coulomb Solids Beyond Original Failure. J. Appl. Mech. 26, 599–602. https://doi.org/10.1115/1.4012119

Johanson, J.R., 1965. A Rolling Theory for Granular Solids. J. Appl. Mech. 32, 842–848. https://doi.org/10.1115/1.3627325

Kleinebudde, P., 2022. Improving Process Understanding in Roll Compaction. J. Pharm. Sci. 111, 552–558. https://doi.org/10.1016/j.xphs.2021.09.024

Kleinebudde, P., 2004. Roll compaction/dry granulation: pharmaceutical applications. Eur. J. Pharm. Biopharm. 58, 317–326. https://doi.org/10.1016/j.ejpb.2004.04.014

Leane, M., Pitt, K., Reynolds, G., Workin, M.C.S.M., 2015. A proposal for a drug product classification system (MCS) for oral solid dosage forms. Pharm Dev. Technol., 20, 12–21. https://doi.org/10.3109/10837450.2014.954728

Mazor, A., Perez-Gandarillas, L., De Ryck, A., Michrafy, A., 2016. Effect of roll compactor sealing system designs: A finite element analysis. Powder Technol. 289, 21–30. https://doi.org/10.1016/j.powtec.2015.11.039

Megarry, A.J., Swainson, S.M.E., Roberts, R.J., Reynolds, G.K., 2019. A big data approach to pharmaceutical flow properties. Int. J. Pharm. 555, 337–345. https://doi.org/10.1016/j.ijpharm.2018.11.059

Muthancheri, I., Rousselin, M., Espinose, A., Sanchez., N., Authelin, J.R., 2024. Modified roller compaction model to account for roll speed effect on powder compaction in dry granulation process. J. Pharm. Sci., 113, 2484–2491. https://doi.org/10.1016/j.xphs.2024.05.006

Nesarikar, V. V., Patel, C., Early, W., Vatsaraj, N., Sprockel, O., Jerzweski, R., 2012. Roller compaction process development and scale up using Johanson model calibrated with instrumented roll data. Int. J. Pharm., 436, 486–507. https://doi.org/10.1016/j.ijpharm.2012.06.027

Pérez Gago, A., Reynolds, G., Kleinebudde, P., 2018. Impact of roll compactor scale on ribbon density. Powder Technol. 337, 92–103. https://doi.org/10.1016/j.powtec.2017.02.045

Reimer, H.L., Kleinebudde, P., 2019. Hybrid modeling of roll compaction processes with the Styl'One Evolution. Powder Technol. 341, 66–74. https://doi.org/10.1016/j.powtec.2018.02.052

Reynolds, G., 2019. Model-based development of roller-compaction processes. In: Chemical engineering in the pharmaceutical industry: Drug product design, development, and modeling, 2nd ed., A, Ende, D. J., Am Ende, M. T. (Eds.), Wiley, Hoboken, NJ, pp.119–145.

Reynolds, G., Ingale, R., Roberts, R., Kothari, S., Gururajan, B., 2010. Practical application of roller compaction process modeling. Comput. Chem. Eng. 34, 1049–1057. https://doi.org/10.1016/j.compchemeng.2010.03.004

Rowe, J.M., Charlton, S.T., McCann, R.J., 2017. Chapter 32 - Development, Scale-Up, and Optimization of Process Parameters: Roller Compaction Theory and Practice, in: Qiu, Y., Chen, Y., Zhang, G.G.Z., Yu, L., Mantri, R.V. (Eds.), Developing Solid Oral Dosage Forms (Second Edition). Academic Press, Boston, pp. 869–915. https://doi.org/10.1016/B978-0-12-802447-8.00032-7

Sato, K., Tanabe, S., Hasegawa, S., Kano, M., 2024. Formulation-independent pharmaceutical dry granulation model via gray box approach, Computer Aided Chemical Engineering, 34 European Symposium on Computer Aided Process Engineering / 15 International Symposium on Process Systems Engineering. Elsevier, pp. 79–84. https://doi.org/10.1016/B978-0-443-28824-1.50014-4

So, C., Leung, L.Y., Muliadi, A.R., Narang, A.S., Mao, C., 2021. Simplifying Johanson's roller compaction model to build a "Virtual Roller Compactor" as a predictive tool – Theory and practical application. Int. J. Pharm. 601, 120579. https://doi.org/10.1016/j.ijpharm.2021.120579

Sun, C.C., Kleinebudde, P., 2016. Mini review: Mechanisms to the loss of tabletability by dry granulation. Eur. J. Phatm. Biopharm., 106, 9–14. https://doi.org/10.1016/j.ejpb.2016.04.003

Tong, Y.L., 1990. The Multivariate Normal Distribution, Springer Series in Statistics. Springer, New York, NY. https://doi.org/10.1007/978-1-4613-9655-0

Toson, P., Lopes, D.G., Paus, R., Kumar, A., Geens, J., Stibale, S., Quodbach, J., Kleinebudde, P., Hsiao, W.-K., Khinast, J., 2019. Model-based approach to the design of pharmaceutical roller-compaction processes. Int. J. Pharm. X 1, 100005. https://doi.org/10.1016/j.ijpx.2019.100005

Zhuang, F., Qi, Z., Duan, K., Xi, D., Zhu, Y., Zhu, H., Xiong, H., He, Q., 2021. A Comprehensive Survey on Transfer Learning. Proc. IEEE 109, 43–76. https://doi.org/10.1109/JPROC.2020.3004555

Zinchuk, A. V., Mullarney, M. P., Hancock, B. C., 2004. Simulation of roller compaction using a laboratory scale compaction simulator. Int. J. Pharm., 269, 403–415. https://doi.org/10.1016/j.ijpharm.2003.09.034

**Highlights**

- Developed a transfer learning approach to predict roller-compactor profiles from compactor-simulator profiles.
- Proposed a generalized correlation to predict the mass correction factor.
- Tested the model on six formulations, improving roller-compactor profile prediction accuracy.
- The mass correction factor was found to be pressure-dependent, not powder-dependent.
- Significantly reduced powder use in early drug development by using a compactor simulator.

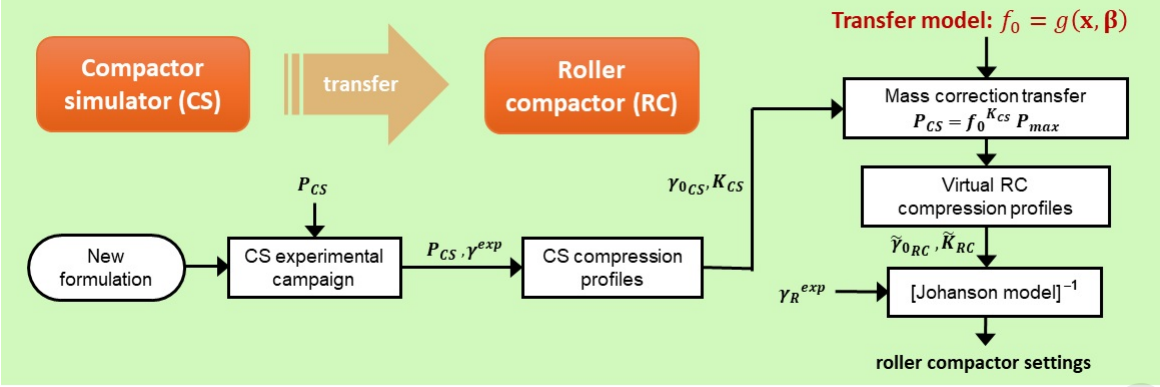

**Declaration of interests**

☐ The authors declare that they have no known competing financial interests or personal relationships that could have appeared to influence the work reported in this paper.

☒ The authors declare the following financial interests/personal relationships which may be considered as potential competing interests:

R.M. Dhenge and F. Cenci are employees of GSK and may hold share options and/or shares in GSK. M.J. Khala was an employee of GSK at the time this study was carried out. The authors declare no other competing conflicts of interest. If there are other authors, they declare that they have no known competing financial interests or personal relationships that could have appeared to influence the work reported in this paper.